The Astrophysical Journal, 640:L163–L166, 2006 April 1

VARIATIONS IN THE SPECTRAL SLOPE OF SAGITTARIUS A* DURING A NEAR-INFRARED FLARE[1]

S. Gillessen,[2] F. Eisenhauer,[2] E. Quataert,[3] R. Genzel,[2,4] T. Paumard,[2] S. Trippe,[2] T. Ott,[2] R. Abuter,[2] A. Eckart,[5] P. O. Lagage,[6] M. D. Lehnert,[2] L. J. Tacconi,[2] and F. Martins[2]

Received 2005 November 10; accepted 2006 February 21; published 2006 March 14

ABSTRACT

We have observed a bright flare of Sgr A* in the near-infrared with the adaptive optics–assisted integral-field spectrometer SINFONI. Within the uncertainties, the observed spectrum is featureless and can be described by a power law. Our data suggest that the spectral index is correlated with the instantaneous flux and that both quantities experience significant changes within less than 1 hour. We argue that the near-infrared flares from Sgr A* are due to synchrotron emission of transiently heated electrons, the emission being affected by orbital dynamics and synchrotron cooling, both acting on timescales of ≈20 minutes.

Subject headings: black hole physics — Galaxy: center — infrared: stars — techniques: spectroscopic

1. INTRODUCTION

The detection of stellar orbits (Schödel et al. 2002; Eisenhauer et al. 2005; Ghez et al. 2003, 2005a) close to Sgr A* has proved that the Galactic center (GC) hosts a massive black hole (MBH), with a mass of $(3.6 \pm 0.2) \times 10^6\ M_\odot$. Sgr A* appears rather dim in all wavelengths, which is explained by accretion flow models (Narayan et al. 1995; Quataert & Narayan 1999; Melia et al. 2000, 2001). In the near-infrared (NIR), Sgr A* was detected only after diffraction-limited observations at 8 m class telescopes became possible (Genzel et al. 2003; Ghez et al. 2004). Usually, the emission is not detectable. However, every few hours Sgr A* flares in the NIR, reaching up to $K \approx 15$ mag. A first flare spectrum was obtained by Eisenhauer et al. (2005), showing a featureless, red spectrum ($\nu S_\nu \sim \nu^\beta$, with $\beta \approx -3$).

2. OBSERVATIONS AND DATA REDUCTION

We observed the GC on 2005 June 18 from 02:40 to 07:15 UT with SINFONI (Eisenhauer et al. 2003; Bonnet et al. 2004), an adaptive optics (AO) assisted integral-field spectrometer mounted at the Cassegrain focus of Unit Telescope 4 (Yepun) of the ESO Very Large Telescope. The field of view was 0.″8 × 0.″8 for individual exposures, mapped onto 64 × 32 spatial pixels. We observed in *K* band with a spectral resolution of FWHM 0.5 nm. The first 12 integrations lasted 5 minutes each. During those we noticed NIR activity of Sgr A* and switched to 4 minute exposures. We followed Sgr A* for another 32 exposures. In total, we interleaved nine integrations on a specifically chosen off field (712″ west, 406″ north of Sgr A*). The seeing was ≈0.″5 and the optical coherence time ≈3 ms, with some short-time deteriorations excluded. The AO was locked on the closest optical guide star ($m_R = 14.65$; 10.″8 east, 18.″8 north of Sgr A*), yielding a spatial resolution of ≈80 mas FWHM, close to the diffraction limit of UT4 in *K* band (≈60 mas).

Our detection triggered immediate follow-up observations with VISIR, a mid-infrared (MIR) instrument mounted at VLT Unit Telescope 3 (Melipal). From 05:25 UT onward, VISIR was pointing to the GC. At the position of Sgr A*, no significant flux was seen. A conservative upper limit of 40 mJy (not dereddened) at 8.59 μm is reported (P. O. Lagage et al. 2006, in preparation).

The reduction of the SINFONI data followed the standard steps: From all source data, we subtracted the respective sky frames to correct for instrumental and atmospheric background. We applied flat-fielding, bad-pixel correction, a search for cosmic-ray hits, and a correction for the optical distortions of SINFONI. We calibrated the wavelength dimension with line emission lamps and tuned on the atmospheric OH lines of the raw frames. Finally, we assembled the data into cubes with a spatial grid of 12.5 mas pixel^{-1}.

3. ANALYSIS

3.1. *Flux Determination*

For all 44 cubes, we extracted a collapsed image (median in spectral dimension) of a rectangular region (0.″25 × 0.″5) centered on Sgr A* and containing the three "S stars" S2, S13, and S17. We determined the flux of Sgr A* from a fit with five Gaussians to each of these images. Four Gaussians with a common width describe the four sources. The fifth Gaussian (with a width 3.5 times wider, typical for the halo from the imperfect AO correction) accounts for the halo of the brightest star, S2 ($K \approx 14$ mag). The halos of the weaker sources (all $K < 15$ mag) could be neglected for the flux measurement. We fixed the positions of all sources (known a priori from a combined cube) and the amplitude ratios for the stars. Five parameters were left free: an overall amplitude, the background, the width, the flux ratio halo/S2, and $\mathcal{F}$, the flux ratio Sgr A*/S2. This procedure disentangles real variability from variations in the background, the Strehl ratio, and the seeing.

As a cross-check, we determined $\mathcal{F}$ in a second way for all images; for both Sgr A* and S2 we measured the flux difference between a signal region centered on-source and a reasonable, symmetric background region. The values thus determined agreed very well with the fits. For further analysis we used the

[1] Based on observations collected at the European Southern Observatory, Paranal, Chile (program 075.B-0547).

[2] Max-Planck-Institut für extraterrestrische Physik, Postfach 1312, D-85741 Garching, Germany.

[3] Department of Astronomy, University of California, Berkeley, 601 Campbell Hall, Berkeley, CA 94720-3411.

[4] Department of Physics, University of California, Berkeley, 366 Le Conte Hall, Berkeley, CA 94720-7300.

[5] I. Physikalisches Institut, Universität zu Köln, Zülpicher Strasse 77, D-50937 Cologne, Germany.

[6] Astrophysique Interactions Multi-échelles, Unité Mixte de Rechercher CEA–CNRS–Université Paris 7, UMR 7158; and Service d'Astrophysique, DAPNIA, Direction des Sciences de la Matière, CEA Saclay, F-91191 Gif-sur-Yvette Cedex, France.

fitted ratios and included the difference between the two estimates in the errors.

3.2. *Choice of Background*

The value of the spectral power law index β crucially depends on the background subtraction. Subtracting too much light would artificially make the signal look redder than it is. Hence, a reasonable choice for the background region excludes the nearby sources S2 and S17. Furthermore, the background flux varies spatially. Actually, Sgr A* lies close to a saddle point in the background light distribution, caused by S2 and S17 (see Fig. 1). In the east-west direction the background has a maximum close to Sgr A*, and in the north-south direction it has a minimum. A proper estimate of the background can be achieved in two ways: (1) working with small enough, symmetric apertures, and (2) subtracting from the signal an off state obtained at the position of Sgr A* from cubes in which no emission is seen. We used the first method, as well as two variants of the second.

Small apertures.—The local background at a position $\boldsymbol{x}$ can be estimated by averaging over a small, symmetric region centered on $\boldsymbol{x}$. Given the background geometry, we have chosen a ring with inner radius 3 pixels and outer radius 7 pixels. The circular symmetry was only broken because we explicitly excluded those pixels with a distance to S17 or S2 smaller than 3 or 7 pixels, respectively. An unfavorable aspect of this method is that the local background is only approximated, since a sufficiently large region has to be declared as signal region.

Off-state subtraction.—The local background can be extracted from cubes in which no signal is seen. Since the seeing conditions change from cube to cube, one still has to correct for the varying amount of stray light in the signal region. We estimate this variation by measuring the difference spectrum between signal and off cube in a stray-light region. The latter must not contain any field stars and should be as far away from the nearby sources as Sgr A*. We used two stray-light regions to the left and to the right of Sgr A*, between 5 and 10 pixels away. The disadvantage of this method is that one needs a suitable off state. The latter point is critical for our data. Even though Sgr A* is not detected directly in the first three cubes, the light at its position appears redder than the local background.[7] Assuming that this light is due to a very dim, red state of Sgr A*, we would subtract too much red light and artificially make the flare too blue. In this sense, this method yields an upper limit for β.

Constant subtraction.—The off-state method can be varied to obtain a lower limit for β. Assuming that the true off-state spectrum has the color of S2, one can demand that it be flat after division by S2. In our data, the S2-divided off-state spectrum is rising toward longer wavelengths. Hence, in this third method we estimate the background at blue wavelengths and use that constant as background for all spectral bins.

3.3. *Determination of Spectral Power Law Index*

We obtained spectra as the median of all pixels inside a disk with radius 3 pixels centered on-source minus the median spectrum of the pixels in the selected off region. In order to correct for the interstellar extinction, we then divided by the S2 spectrum (obtained in the same way as the signal). Next, the temperature of S2 was corrected by multiplying by the value of νS_ν for a blackbody with $T \approx 25{,}000$ K. After binning the data into 60 spectral channels, they are finally fitted with a power law $\sim \nu^\beta$. With this definition, red emission has $\beta < 0$. The error on β is obtained as the square sum of the formal fit error and the standard deviation in a sample of 20 estimates for β obtained by varying the on- and off-region selection.

[7] Inspecting older (nonflare) SINFONI data, we found cases similar to the new data and other cases in which the light was identical to the local background emission. This is consistent with the *L*-band observations by Ghez et al. (2004, 2005b).

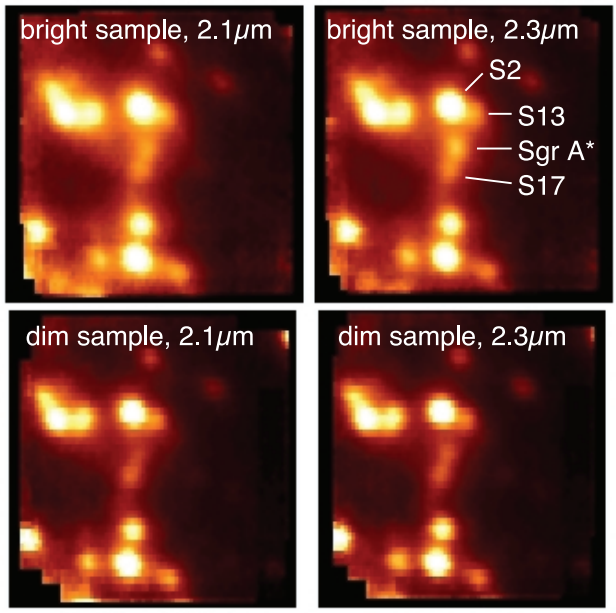

FIG. 1.—The Galactic center as seen with SINFONI. Shown are channel maps from the bright and the dim sample, obtained by taking the mean in spectral dimension from 2.05 to 2.15 μm and from 2.25 to 2.35 μm. All images are scaled in the same way and use an identical color map. Sgr A* is brighter in the longer wavelength maps, indicating that it is redder than the field stars. Furthermore, the effect is more pronounced in the dim sample, meaning that Sgr A* is redder therein than in the bright sample.

4. RESULTS

We observed a strong (flux density up to 8 mJy, or $\nu L_\nu \approx 10^{35}$ ergs s^{-1}), long (>3 hr) flare that showed significant brightness variations on timescales as short as 10 minutes (Fig. 2, *top*). While the data are not optimal for a periodicity search (poorer sampling than our previous imaging data), it is worth noting that the highest peak in the periodogram (significance of $\approx 2\ \sigma$) lies at a period of $\approx$18 minutes. This is also the timescale found by Genzel et al. (2003), who identify the quasi periodicity with the orbital time close to the last stable orbit (LSO) of the MBH.

We divided the data into three groups: (1) the cubes for the first peak, near $t = 50$ minutes ("preflare"), (2) the cubes at $t > 100$ minutes with $\mathcal{F} < 0.25$ ("dim state"), and (3) the cubes at $t > 100$ minutes with $\mathcal{F} > 0.25$ ("bright state"). For the three sets, we created combined cubes in which we determined β using all three background estimates. In all cases we obtained the correct spectral index of 2.9 ± 0.5 for S17 (a star with a spectrum similar to S2 but a flux comparable to Sgr A*). For Sgr A* we find the results shown in Table 1.

The values obtained from the small apertures lie between the values from the other two methods, consistent with the idea that they yield upper and lower limits. The absolute values vary systematically according to the chosen background method.

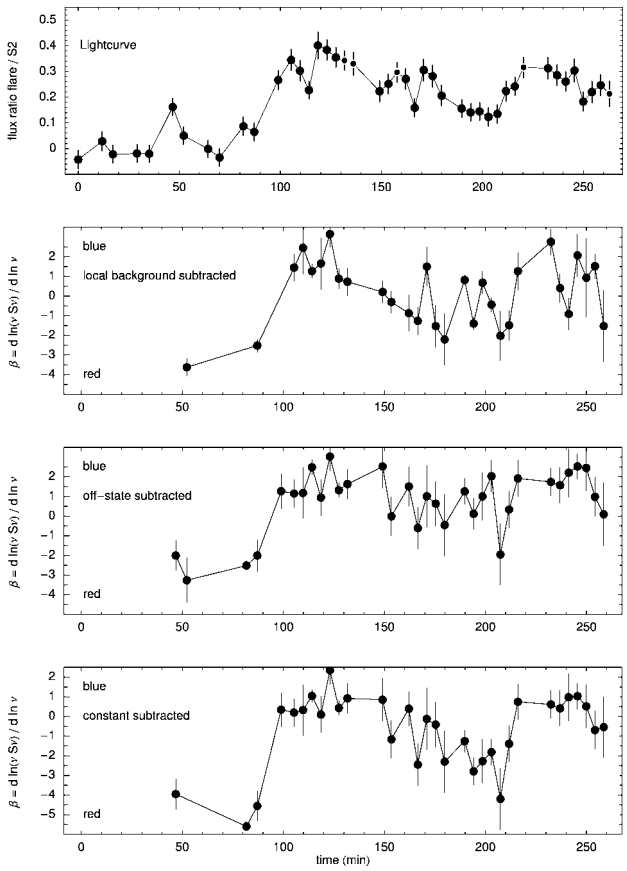

FIG. 2.—Light curve and variation of the spectral power law index β during the flare. Time is counted from 02:40 UT. *Top*, flux ratio flare/S2 (smaller points are exposures affected by bad seeing); *upper middle*, β using the small-apertures background; *lower middle*, β using the off-state subtraction background; *bottom*, β using the constant subtraction background.

However, independent of that, it is clear that the preflare is redder than the dim state, which in turn is redder than the bright state. An obvious question then is whether flux and β are directly correlated.

Hence, we applied the spectral analysis to the individual cubes. We kept the data in which Sgr A* is detected, the error $\Delta\beta < 1.5$, and the spectral index for S17 does not deviate more than 1.5 from the expected value. The resulting spectral indices appear to be correlated with the flux (Figs. 2 and 3). The values

TABLE 1

RESULTS FOR SPECTRAL POWER LAW INDEX β

Method	Preflare	Dim State	Bright State
Off-state subtraction	-1.4 ± 0.4	-0.7 ± 0.4	$+0.4 \pm 0.2$
Small apertures	-1.8 ± 0.3	-1.7 ± 0.4	-0.1 ± 0.3
Constant subtraction	-3.4 ± 0.4	-2.3 ± 0.3	-0.3 ± 0.2

match the results of Eisenhauer et al. (2005) and Ghez et al. (2005b). Bright flares are indeed bluer than weak flares, as suspected by Ghez et al. (2005b) and consistent with the earlier multiband observations of Genzel et al. (2003). Our key new result is that this holds even within a single event.

For all three background methods, it is clear that the main event was preceded by a weak red event. For the small apertures and the constant subtraction method, instantaneous flux and spectral index are correlated. For the off-state subtraction method, one could instead group the data into a preflare at the beginning and a bluer, brighter main event.

We checked our data for contamination effects. If stray light had affected the flare signal, β should be correlated with the seeing (measured by the width from the multiple fits). Since we did not find such a correlation, we exclude significant contamination.

5. INTERPRETATION

Theoretical models predict that the millimeter/IR emission from Sgr A* is synchrotron emission from relativistic electrons close to the LSO (Liu & Melia 2001; Quataert 2003; Liu et al. 2004, 2006). Radiatively inefficient accretion flow (RIAF) models with a thermal electron population ($T_e \approx 10^{11}$ K) produce the observed peak in the submillimeter but fail to produce enough flux at 2 μm. The NIR emission requires transiently heated or accelerated electrons, as proposed by Markoff et al. (2001).

A conservative interpretation of our data is suggested by Figure 3 (*middle*). There was a weak, red event before and possibly independent of the main flare, which was a much bluer event. Plausibly, the preflare is then due to the high-energy tail of the submillimeter peak (Genzel et al. 2003). The main flare nevertheless requires a population of heated electrons.

A more progressive interpretation follows from the correlation between flux and β (Fig. 3, *left and right*). This suggests that the NIR variability is caused by the combination of transient heating with subsequent cooling and orbital dynamics of

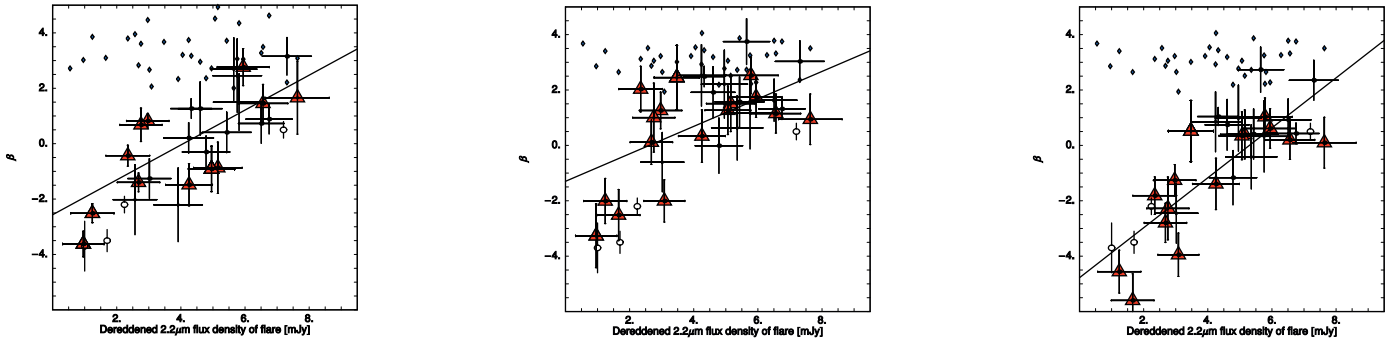

FIG. 3.—Correlation plots between the flare flux and the spectral index β. Points with error bars represent the flare, and blue dots are β_{S17}. Filled circles mark points with error $\Delta\beta < 1$, and red triangles mark the data with good seeing (FWHM < 75 mas). The lines are fits to the filled circles. Open circles indicate the data from Eisenhauer et al. (2005; near 2 mJy) and Ghez et al. (2005b; near 7 mJy). *Left*, small-apertures method; *middle*, off-state subtraction method; *right*, constant subtraction method.

relativistic electrons. In the following subsections, we will exploit this idea.

5.1. *Synchrotron Emission*

In the absence of continued energy injection, synchrotron cooling will suppress the high-energy part of the electron distribution function. This results in a strong cutoff in the NIR spectrum with a cutoff frequency decreasing with time. At a fixed band, one expects the light to become redder as the flux decreases. This can cause a correlation between flux and β. The observed flare apparently needs several heating and cooling events.

The synchrotron cooling time is comparable to the observed timescale of decaying flanks as in Figure 2 (*top*) or Genzel et al. (2003). In an RIAF model (Yuan et al. 2003), the magnetic field B is related to the accretion rate $\dot{M}$. For disk models with $\dot{M} \approx 10^{-8}\ M_{\odot}\ \mathrm{yr}^{-1}$ (Agol 2000; Quataert & Gruzinov 2000), one has $B \approx 30$ G at a radial distance of $3.5R_{\mathrm{S}}$ (Schwarzschild radii). The cooling time for electrons emitting at $\lambda = 2\lambda_2\ \mu$m for $B = 30B_{30}$ G is

$$t_{\mathrm{cool}} \approx 8B_{30}^{-3/2}\lambda_2^{1/2}\ \mathrm{minutes}. \qquad (1)$$

This is similar to the orbital timescale, making it difficult to disentangle flux variations due to heating and cooling from dynamical effects due to the orbital motion.

5.2. *Orbital Dynamics*

The timescale of ≈20 minutes for the observed variations suggests orbital motion close to the LSO as one possible cause. Any radiation produced propagates through strongly curved spacetime. Beaming, multiple images, and Doppler shifts have to be considered (Hollywood et al. 1995; Hollywood & Melia 1997). Recent progress has been made in simulating these effects when observing a spatially limited emission region orbiting the MBH (Paumard et al. 2005; Broderick & Loeb 2005, 2006a, 2006b).

That the emission region is small compared with the accretion disk can be deduced from X-ray observations. Eckart et al. (2004, 2006) report similar timescales for X-ray and IR flares. This excludes the X-ray emission from being synchrotron light, as one would expect cooling times under 1 minute (eq. [1]). The X-ray emission is naturally explained by inverse Compton (IC) scattering of the transiently heated electrons, which have a Lorentz factor of $\gamma \approx 10^3$. The IC process scatters the seed photon field up according to $\nu_{\mathrm{IC}} \approx \gamma^2\nu_{\mathrm{seed}}$. Given $\nu_{\mathrm{IC}} \approx 10^{18}$ Hz for X-rays, the seed photon frequency is $\nu_{\mathrm{seed}} \approx 10^{12}$ Hz—the submillimeter regime. The X-ray intensity for the synchrotron self-Compton case is given by

$$\mathrm{X/IR} = L_{\mathrm{SSC}}/L_{\mathrm{sync}} \approx 10^{-2}L_{35}(R/R_{\mathrm{S}})^{-2}B_{30}^{-2}, \qquad (2)$$

where L_{35} is the seed photon field luminosity in units of 10^{35} ergs s^{-1} and R is the radius of the emission region. The highest value of L_{35} compatible with the MIR and submillimeter data is reached for a flat spectrum ($\beta = 0$) of the heated electrons. Thus, $L_{35} \lesssim 1$. Using equation (2), we have $R/R_{\mathrm{S}} \approx 0.1[L_{35}/(\mathrm{X/IR})]^{1/2}$. From the observed ratios X/IR ≈ 0.1–1, we derive $R < 0.3R_{\mathrm{S}}$. This means that the emission region has to be a small spot.

A plausible dynamical model is discussed by T. Paumard et al. (2006, in preparation). It reproduces typical light curves as observed by Genzel et al. (2003) or in Figure 2. Because of the Doppler effect, the observed light corresponds to different rest-frame frequencies, depending on the orbital phase. If the source spectrum is curved, flux and spectral index appear correlated. Following this interpretation, the emission during the brightest part of the flare originates from a rest frequency with larger β than the dimmer state, which is emitted at shorter wavelengths. Such a concavely curved spectrum is naturally expected from the synchrotron models.

REFERENCES

Agol, E. 2000, ApJ, 538, L121
Bonnet, H., et al. 2004, Messenger, No. 117, 17
Broderick, A. E., & Loeb, A. 2005, MNRAS, 363, 353
———. 2006a, ApJ, 636, L109
———. 2006b, MNRAS, in press (astro-ph/0509237)
Eckart, A., et al. 2004, A&A, 427, 1
———. 2006, A&A, in press (astro-ph/0512440)
Eisenhauer, F., et al. 2003, Proc. SPIE, 4841, 1548
———. 2005, ApJ, 628, 246
Genzel, R., Schödel, R., Ott, T., Eckart, A., Alexander, T., Lacombe, F., Rouan, D., & Aschenbach, B. 2003, Nature, 425, 934
Ghez, A., Salim, S., Hornstein, S., Tanner, A., Lu, J., Morris, M., Becklin, E. E., & Duchêne, G. 2005a, ApJ, 620, 744
Ghez, A., et al. 2003, ApJ, 586, L127
———. 2004, ApJ, 601, L159
———. 2005b, ApJ, 635, 1087
Hollywood, J. M., & Melia, F. 1997, ApJS, 112, 423
Hollywood, J. M., Melia, F., Close, L. M., McCarthy, D. W., Jr., & Dekeyser, T. A. 1995, ApJ, 448, L21
Liu, S., & Melia, F. 2001, ApJ, 561, L77
Liu, S., Melia, F., & Petrosian, V. 2006, ApJ, 636, 798
Liu, S., Petrosian, V., & Melia, F. 2004, ApJ, 611, L101
Markoff, S., Falcke, H., Yuan, F., & Biermann, P. L. 2001, A&A, 379, L13
Melia, F., Liu, S., & Coker, R. 2000, ApJ, 545, L117
———. 2001, ApJ, 553, 146
Narayan, R., Yi, I., & Mahadevan, R. 1995, Nature, 374, 623
Paumard, T., et al. 2005, Astron. Nachr., 326, 568
Quataert, E. 2003, Astron. Nachr., 324(S1), 435
Quataert, E., & Gruzinov, A. 2000, ApJ, 539, 809
Quataert, E., & Narayan, R. 1999, ApJ, 520, 298
Schödel, R., et al. 2002, Nature, 419, 694
Yuan, F., Quataert, E., & Narayan, R. 2003, ApJ, 598, 301